Journal of Molecular Structure 1154 (2018) 392–405

Contents lists available at ScienceDirect

Journal of Molecular Structure

journal homepage: http://www.elsevier.com/locate/molstruc

Evaluation of the structural properties of powerful pesticide dieldrin in different media and their complete vibrational assignment

María V. Castillo [a], Maximiliano A. Iramain [a], Lilian Davies [b], María E. Manzur [a], Silvia Antonia Brandán [a, *]

[a] Cátedra de Química General, Instituto de Química Inorgánica, Facultad de Bioquímica, Química y Farmacia, Universidad Nacional de Tucumán, Ayacucho 471, 4000, San Miguel de Tucumán, Tucumán. R, Argentina
[b] Instituto de Investigaciones para la Industria Química (INIQUI, CONICET), Universidad Nacional de Salta, Av. Bolivia 5150, 4400, Salta, Argentina

ARTICLE INFO

Article history:
Received 18 September 2017
Received in revised form
16 October 2017
Accepted 17 October 2017
Available online 20 October 2017

Keywords:
Dieldrin
Vibrational spectra
Molecular structure
Force field
DFT calculations

ABSTRACT

Dieldrin was characterized by using Fourier Transform infrared (FT-IR) and Raman (FT-Raman), Ultraviolet–Visible (UV–Visible) spectroscopies. The structural and vibrational properties for dieldrin in gas phase and in aqueous solution were computed combining those experimental spectra with hybrids B3LYP and WB97XD calculations by using the 6-31G* and 6-311++G** basis sets. Here, the experimental available Hydrogen and Carbon Nuclear Magnetic Resonance (^{1}H and ^{13}C NMR) for dieldrin were also used and compared with those predicted by calculations. The B3LYP/6-311++G** method generates the most stable structures while the results have demonstrated certain dependence of the volume and dipole moment values with the method, size of the basis set and, with the studied media. The lower solvation energy for dieldrin (−32.94 kJ/mol) is observed for the higher contraction volume (−2.4 Å^3) by using the B3LYP/6-31G* method. The NBO studies suggest a high stability of dieldrin in gas phase by using the WB97XD/6-31G* method due to the $n \rightarrow \pi^*$ and $n^* \rightarrow \pi^*$ interactions while the AIM analyses support this high stability by the C18···H26 and C14···O7 contacts. The different topological properties observed in the R5 ring suggest that probably this ring plays a very important role in the toxics properties of dieldrin. The frontier orbitals show that when dieldrin is compared with other toxics substances the reactivity increases in the following order: CO < STX < dieldrin < C_6Cl_6 <TCAB < TCAOB < CN^- where evidently, the presence of five rings and six Cl atoms decrease the reactivity of dieldrin, as compared with hexachlorobencene. The WB97XD method and the two basis sets predicted for dieldrin in both media low reactivities, higher nucleophilicity and, low electrophilicity. All the bands observed in the IR and Raman spectra were completely assigned to the 75 vibration normal modes and their harmonic force fields and force constants for first time are reported for dieldrin. The predicted FTIR, FT-Raman, UV–Visible and ^{1}H and ^{13}C NMR spectra for dieldrin show a reasonable concordance with the experimental ones.

1. Introduction

Dieldrin is an organochlorine compound whose IUPAC name and molecular formula are respectively (1R,4S,4aS,5R,6R,7S,8-S,8aR)-1,2,3,4,10,10- hexachloro-6,7-epoxy-1,4,4a,5,6,7,8,8a-octahydro-1,4:5,8- dimethanonaphthalene and $C_{12}H_8Cl_6O$. Due to the presence of six Cl atoms in their structure it is widely used as insecticide and pesticide, for which confers to it toxicological properties [1–18]. Hence, all studies related with this organochlorine compound are of great importance principally to the environmental and the health human [1,3,5–8,10–13,16–18]. In this senses, the man is exposed mainly by the dietary intake of food of animal and vegetal origin [10,11] and, for these reasons, all the multiple effects associated with that pesticide are strongly dependent on duration and the length and time of exposure [11]. Consequently, it stimulates the nervous system causing hyperexcitation neurotoxic, and seizures including cancer [11]. Recent studies reported by Allen et al. [13] have correlated the environmental exposure to dieldrin pesticide with the incidence of Parkinson's disease (PD). Experimentally, the detection of dieldrin, due to their characteristics toxics, is normally performed by using infrared and Raman spectroscopies [4,7,8,14,16] because both are

* Corresponding author.
E-mail address: sbrandan@fbqf.unt.edu.ar (S.A. Brandán).

https://doi.org/10.1016/j.molstruc.2017.10.065
0022-2860/

useful techniques to analyze trace samples and to highlight those studies by Surface-enhanced Raman spectroscopy (SERS) due to the fact that it is a very important tool to detect little quantity adsorbed of dieldrin on different surfaces [14,16]. So far, there are not complete assignments of all bands observed in their vibrational spectra in order to completely identify this substance in all the media in which it can be found. In this context, the aim of this work is to study, first, their most stable structure in gas and aqueous solution phases by using the hybrid B3LYP method [19,20] and the functional which include long range corrections such as the WB97XD method [21] and the 6-31G* and 6-311++G** basis sets while in solution the solvent effects were studied with the PCM and SD models [22–24]. Hence, their structural properties can be determined and, after that, to perform the complete assignments of all the bands observed in both experimental infrared and Raman spectra by using their internal normal coordinates and the Scaled Quantum Mechanical Force Field (SQMFF) approach [25]. Their harmonic force constants were also determined from their corresponding harmonic force fields and by using the Molvib program [26]. On the other hand, as mentioned by Allen et al. [13] the concentration of pesticides affects cellular processes associated with PD patients and, so far, the mechanism and specific cellular targets have not been fully elucidated. For these reasons, the frontier orbitals [27,28] and some interesting descriptors [29–32] were also studied in this work by using both methods because these parameters are essential to predict their reactivities and behaviour in any media due to that it is necessary to know and understand the mechanisms of action and role of dieldrin as a toxic agent. Then, these descriptors were compared with other reported results for compounds with different biological properties from toxic substances up to antiviral agents [32–38].

2. Experimental

The substance dieldrin used to record the IR spectrum was a pure anhydrous (Riedel de Haën) commercial sample. For this reason, the spectrum of the solid sample was recorded in KBr pellets (2 mg of solid sample in 200 mg of KBr) in the 4000-400 cm^{-1} range with an FT-IR Perkin Elmer spectrophotometer, provided with a Globar source and DGTS detector. The Raman spectra of the substance in solid state was recorded in the 4000-100 cm^{-1} range with a Bruker RF100/S spectrometer equipped with a Nd:YAG laser (excitation line of 1064 nm, 800 mW of laser power) and a Ge detector cooled at liquid nitrogen temperature. Both IR and Raman spectra were recorded with a resolution of 1 cm^{-1} and 200 scans.

A Beckman spectrophotometer was used to record the ultraviolet–visible spectrum in $CHCl_3$ solution from 200 up to 500 nm.

3. Computational details

The initial 3D structure of dieldrin was taken from Ref. [39], modelled with the *GaussView* program [40] by using the hybrid B3LYP and WB97XD methods [19–21], where the latter method includes empirical dispersion and then, these structures were optimized with the Gaussian 09 program [41] and the 6-31G* and B3LYP/6-311++G** basis sets. Dieldrin has five fused rings of which one of them has three members, other three rings have five members and, there is only one ring with six members. The definition of these rings can be clearly seen in Fig. 1 while the dieldrin structure together with the atoms labeling is presented in Fig. 2. In this work, we have studied two different charges taking into account the presence of six Cl atoms in the dieldrin structure, these are, the atomic natural population charges (NPA) computed by using the NBO program [42] and, the Merz-Kollman (MK) charges

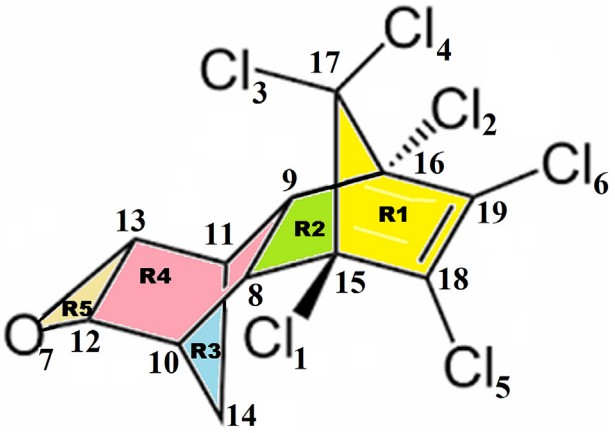

Fig. 1. Perspective view of the molecule of dieldrin with the identifications of their five different rings.

[43]. With these latter charges the molecular electrostatic potential were also calculated. The characteristics of different bonds and interactions were predicted by means of the bond orders, the donor-acceptor interactions and the topological properties which were computed with the NBO calculations [42] and the AIM2000 program [44] by using the Bader's theory [45]. The HOMO-LUMO orbitals were calculated to investigate the reactivities of dieldrin in the different media and from the differences between both orbitals, these are the gap values, their reactivities were also predicted [27,28]. Later, by using these gap values the chemical potential (μ), electronegativity (χ), global hardness (η), global softness (S) and global electrophilicity index (ω) parameters were calculated with known equations [29–32] by using both levels of theory.

The complete assignments of all bands observed in the experimental infrared and Raman spectra were performed by using the harmonic force fields computed to both levels of theory with the SQMFF methodology [25], the Molvib program [26] and, by using the normal internal coordinates. Here, it is necessary to clarify that three rings coordinates were removed, as a consequence of the five fused rings that has dieldrin, in similar form that were built the coordinates for tropane, cocaine and morphine alkaloids [36,37,46].

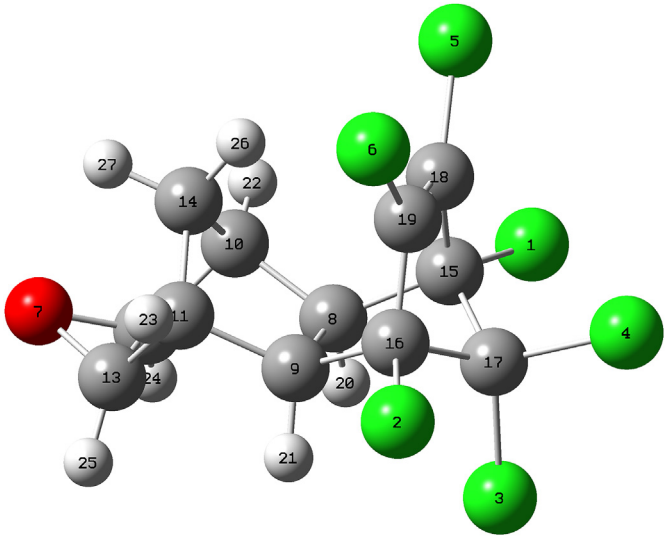

Fig. 2. Molecular theoretical structure of dieldrin and the atoms numbering.

Then, the vibrational assignments were performed taking into account those potential energy distribution (PED) contributions $\geq$ 10%. At this point, the properties of dieldrin were compared with other chlorinated compounds with different properties [32,36,37,46].

4. Results and discussion

4.1. Structural study

Calculated total energies, dipolar moments, solvation energy and volume values for dieldrin in gas phase and, in aqueous and ethanol solution by using the two B3LYP and WB97XD methods [19–21] with the 6-31G* and 6-311++G** basis sets can be seen in Table 1. Here, the volume values were calculated with the Moldraw program [47]. The detailed analysis of the results shows that: (i) the B3LYP/6-311++G** method generate the most stable structures for dieldrin in all media, (ii) the higher dipole moment values are observed with the WB97XD/6-31G* method in both media and, (iii) the B3LYP method predicted the higher volume in gas phase by using the 6-31G* basis set and in aqueous solution by using the higher size basis set. In Fig. S1 (supporting material) we clearly observed the influence of both methods and basis sets on the dipole moment and volume values of dieldrin in gas and aqueous solution phases. Hence, the dipole moment presents higher values in solution and the highest values are observed with both methods by using the 6-31G* basis set while when in the volumes, the same behaviour is analyzed and is observed with both methods by using the 6-311++G** basis set in both media but when the B3LYP/6-31G* method is used the values in both media notably change presenting the higher volume value in gas phase. Probably, for this reason the higher volume variation in solution (−2.4 Å^3) is observed with this method. In relation to the solvation energy, the B3LYP/6-311++G** method predicted the higher value for the lower volume contraction.

The experimental structure of dieldrin was not reported so far, and, for this reason, their calculated geometrical parameters in gas phase for those two methods and two basis sets are summarized in Table 2. These results were compared with those experimental obtained by X-ray diffraction for 1,2,3,4,10,10-hexaehloro-1,4,4a,5,8,8a-hexahydro-*endo*-1,4-*endo*-5,8-dimethanonaphthalene (Isodrin) [48] and dimethyl 1,2,3,4,7,7-hexachloro-5-*endo*-methoxybicyclo[2.2.1]hept-2-ene-5-exo,6-*endo*-dicarboxylate [49] by means of the root-mean-square deviation (RMSD) values which were included in Table 2. The concordance between the theoretical and experimental values with both methods and basis sets are reasonable when they are compared with the two compounds because these calculations show rmsd values between 2.6 and 2.7 Å for bond lengths and 3.4–3.2° for bond angles but the better values are evidently obtained when the bond lengths and angles are compared with those experimental observed for isodrin [48].

4.2. NPA and MK charges, MEP and bond orders (BO)

Taking into account the toxicological properties of dieldrin and the presence of six Cl atoms in their structure [1,3,5,13,14] it is very important to analyze different types of charges and their distributions by means of the molecular electrostatic potentials (MEP) values and their surfaces mapped. Hence, we have analyzed the MK and NPA charges, the molecular electrostatic potential (MEP) and the bond orders, expressed as Wiberg indexes, by using the two methods and basis sets and in gas and aqueous solution phases. In Table S1 the MK and NPA charges are summarized and predicted for dieldrin while in Table S2 Wiberg indexes are given the and, in Table S3 the MEP values. In Fig. S2 the influence of B3LYP and WB97XD methods [19–21] and 6-31G* 6-311++G** basis sets on the MK charges are presented for dieldrin in gas phase while in Fig. S3 the variations of these charges for dieldrin are shown in both media. The same MK variations on all atoms are practically observed in Fig. S2 with both methods by using the 6-311++G** basis set while different behaviour is observed on all atoms with both methods when the 6-31G* basis set is used showing the lower values on the C9 and C17 atoms by using the WB97XD method. The low values on these latter atoms are probably justified because they belong to the CCl_2 groups where the two Cl3 and Cl4 atoms involved present the higher positive values, as observed in Fig. S2 and S3.

The comparisons between the MK and NPA charges by means of graphics can be seen in Fig. S4 where it is possible to observe clearly that the behaviour of both charges with the different methods are completely different, thus, the NPA charges with both methods and basis sets present practically the same behaviour, however, the MK charges by using the two B3LYP and WB97XD methods and the 6-31G* basis set have different behaviour from that observed by using 6-311++G** basis set. Hence, these results show that both methods and set basis have notable effects on the MK charges than the NPA charges.

In relation to the BO, we observed that in both media the B3LYP method predicted values slightly higher than the WB97XD method,

Table 1
Calculated total energy (*E*), dipolar moments, solvation energy and volume values for Dieldrin in different media.

Property	GAS PHASE			
	6-31G* Basis set		6-311++G** Basis set	
	B3LYP	WB97XD	B3LYP	WB97XD
E (Hartrees)	−3298.3747	3298.1535	−3298.6826	3298.4482
μ (D)	1.70	1.75	1.47	1.50
V (Å^3)	294.6	292.4	294.1	292.3
Property	AQUEOUS SOLUTION/PCM			
	B3LYP	WB97XD	B3LYP	WB97XD
E (Hartrees)	−3298.3820	−3298.1612	−3298.6915	−3298.4568
μ (D)	2.55	2.61	2.43	2.47
V (Å^3)	292.2	293.0	293.6	291.5
Solvation energies (kJ/mol) and volume variations				
Methods	ΔG_{un}	ΔG_{ne}	$\Delta G_{corrected}$	ΔV(Å^3)
B3LYP/6-31G*	−19.15	13.79	−32.94	−2.4
WB97XD/6-31G*	−20.20	13.67	−33.87	0.6
B3LYP/6-311++G**	−23.34	13.75	−37.09	−0.5
WB97XD/6-311++G**	−22.56	13.63	−36.19	−0.8

Table 2
Calculated geometrical parameters for the Dieldrin in gas phase.

Parameter	B3LYP[a]		Wb97xd[a]		Exp[b]	Exp[c]
	6-31G*	6-311++G**	6-31G*	6-311++G**		
Bond Length (Å)						
Cl1–C15	1.780	1.779	1.766	1.765	1.745	1.74
Cl2–C16	1.780	1.779	1.766	1.765	1.749	1.74
Cl3–C17	1.798	1.796	1.782	1.781	1.775	1.75
Cl4–C17	1.793	1.792	1.778	1.778	1.771	1.86
Cl5–C18	1.714	1.713	1.705	1.704	1.689	1.70
Cl6–C19	1.714	1.713	1.705	1.704	1.702	1.69
O7–C12	1.435	1.434	1.422	1.420		
O7–C13	1.435	1.434	1.422	1.421		
C8–C9	1.578	1.577	1.568	1.566	1.566	1.53
C8–C10	1.558	1.557	1.551	1.549		1.59
C8–C15	1.565	1.562	1.557	1.554	1.607	1.57
C8–H20	1.093	1.090	1.093	1.091		1.09
C9–C11	1.558	1.557	1.551	1.549	1.527	1.64
C9–C16	1.565	1.563	1.557	1.554	1.548	1.58
C9–H21	1.093	1.090	1.093	1.091		1.05
C10–C12	1.544	1.543	1.539	1.537		
C10–C14	1.545	1.544	1.539	1.538		
C10–H22	1.092	1.089	1.091	1.089		1.02
C11–C13	1.544	1.543	1.539	1.537		
C11–C14	1.545	1.544	1.539	1.538		
C11–H23	1.092	1.089	1.091	1.089		0.97
C12–C13	1.474	1.472	1.468	1.467		
C12–H24	1.088	1.085	1.087	1.085		
C13–H25	1.088	1.085	1.087	1.085		
C14–H26	1.085	1.082	1.084	1.082		
C14–H27	1.090	1.088	1.090	1.088		
C15–C17	1.578	1.576	1.570	1.567	1.536	1.48
C15–C18	1.527	1.526	1.521	1.520	1.535	1.43
C16–C17	1.578	1.576	1.570	1.567	1.544	1.51
C16–C19	1.527	1.526	1.521	1.520	1.515	1.46
C18 = C19	1.341	1.337	1.335	1.331	1.310	1.34
RMSD[a]	**0.027**	**0.026**	**0.021**	**0.021**		
RMSD[b]	**0.060**	**0.059**	**0.058**	**0.057**		
Bond angle (degrees)						
C9–C8–C10	103.1	103.1	103.2	103.2		
C9–C8–C15	102.8	102.8	102.8	102.8	110.0	104.7
C9–C8–H20	111.5	111.5	111.7	111.6		
C10–C8–C15	122.3	122.3	121.9	122.0		124.3
C10–C8–H20	110.3	110.3	110.2	110.3		
C15–C8–H20	106.4	106.4	106.7	106.7		
C8–C9–C11	103.1	103.1	103.2	103.2		100.1
C8–C9–C16	102.8	102.7	102.8	102.8	104.6	103.5
C8–C9–H21	111.5	111.5	111.7	111.6		
C11–C9–C16	122.3	122.4	121.9	122.0	113.4	127.0
C11–C9–H21	110.3	110.4	110.2	110.3		
C16–C9–H21	106.4	106.4	106.7	106.7		
C8–C10–C12	100.8	100.8	100.5	100.5		
C8–C10–C14	104.6	104.5	104.8	104.7		
C8–C10–H22	115.4	115.5	115.4	115.4		
C12–C10–C14	100.2	100.4	100.2	100.4		
C12–C10–H22	116.1	116.0	116.3	116.2		
C14–C10–H22	117.3	117.4	117.3	117.4		
C9–C11–C13	100.8	100.8	100.5	100.5		
C9–C11–C14	104.6	104.4	104.8	104.7		
C9–C11–H23	115.4	115.5	115.4	115.4		
C13–C11–C14	100.2	100.4	100.2	100.4		
C13–C11–H23	116.1	116.0	116.3	116.2		
C14–C11–H23	117.3	117.4	117.3	117.4		
O7–C12–C10	116.2	116.2	116.3	116.2		
O7–C12–H24	116.0	115.9	116.2	116.2		
C10–C12–C13	105.2	105.2	105.2	105.2		
C10–C12–H24	121.2	121.3	121.1	121.1		
C13–C12–H24	123.8	123.9	123.7	123.8		
O7–C13–C11	116.2	116.1	116.3	116.2		
O7–C13–H25	116.0	115.9	116.2	116.2		
C11–C13–C12	105.2	105.3	105.2	105.2		
C11–C13–H25	121.2	121.2	121.1	121.1		
C12–C13–H25	123.8	123.9	123.7	123.8		
C10–C14–C11	95.4	95.3	95.3	95.3		

(*continued on next page*)

Table 2 (*continued*)

Parameter	B3LYP[a]		Wb97xd[a]		Exp[b]	Exp[c]
	6-31G*	6-311++G**	6-31G*	6-311++G**		
C10–C14–H26	115.0	114.9	115.2	115.1		
C10–C14–H27	111.3	111.5	111.3	111.4		
C11–C14–H26	115.0	114.8	115.2	115.1		
C11–C14–H27	111.3	111.5	111.3	111.5		
H26–C14–H27	108.4	108.4	108.1	108.1		
Cl1–C15–C8	114.0	114.2	114.1	114.2	117.6	112.0
Cl1–C15–C17	116.2	116.1	116.3	116.2	116.4	118.2
Cl1–C15–C18	115.6	115.6	115.7	115.6	114.0	116.2
C8–C15–C17	100.5	100.5	100.7	100.6	102.8	96.8
C8–C15–C18	110.1	110.1	109.7	109.7	104.6	108.9
C17–C15–C18	98.3	98.4	98.5	98.5	99.3	103.7
Cl2–C16–C9	114.0	114.2	114.1	114.2	114.1	111.9
Cl2–C16–C17	116.2	116.1	116.3	116.2	116.0	117.9
Cl2–C16–C19	115.6	115.6	115.7	115.6	116.5	119.1
C9–C16–C17	100.6	100.5	100.7	100.6	99.9	93.4
C9–C16–C19	110.1	110.2	109.7	109.7	109.4	109.5
C17–C16–C19	98.3	98.3	98.5	98.5	98.7	101.7
Cl3–C17–Cl4	107.2	107.1	107.5	107.4	107.0	107.6
Cl3–C17–C15	114.4	114.4	114.3	114.3	113.3	119.3
Cl3–C17–C16	114.4	114.5	114.3	114.4	113.7	116.4
Cl4–C17–C15	114.3	114.3	114.2	114.2	113.9	109.2
Cl4–C17–C16	114.3	114.3	114.2	114.2	115.4	108.2
C15–C17–C16	92.0	92.0	92.0	92.1	93.4	95.3
Cl5–C18–C15	124.3	124.3	124.2	124.2	124.5	127.7
Cl5–C18–C19	127.7	127.6	127.8	127.7	128.3	124.2
C15–C18–C19	107.7	107.7	107.7	107.7	107.2	108.1
Cl6–C19–C16	124.3	124.3	124.2	124.2	123.8	124.4
Cl6–C19–C18	127.7	127.6	127.8	127.7	127.8	128.6
C16–C19–C18	107.7	107.8	107.7	107.7	108.3	107.0
RMSD[a]	**2.7**	**2.7**	**2.6**	**2.6**		
RMSD[b]	**3.2**	**3.3**	**3.4**	**3.4**		
Diedral angles (degrees)						
C10–C8–C9–C11	0.0	0.2	0.0	0.0		
C10–C8–C9–C16	−128.0	−127.9	−127.6	−127.6		
C10–C8–C9–H21	118.3	118.5	118.3	118.4		
C15–C8–C9–C11	128.0	128.2	127.6	127.7		
C15–C8–C9–C16	0.0	0.1	0.0	0.1		
C15–C8–C9–H21	−113.7	−113.5	−114.1	−113.9		
H20–C8–C9–C11	−118.4	−118.2	−118.3	−118.3		
H20–C8–C9–C16	113.6	113.8	114.1	114.0		
H20–C8–C9–H21	0.0	0.2	0.0	0.1		
C9–C8–C10–C12	−71.4	−71.5	−71.5	−71.5		
C9–C8–C10–C14	32.3	32.3	32.1	32.2		
C9–C8–C10–H22	162.7	162.7	162.6	162.7		
C15–C8–C10–C12	174.0	173.9	174.0	174.0		
C15–C8–C10–C14	−82.3	−82.3	−82.4	−82.3		
C15–C8–C10–H22	48.1	48.1	48.1	48.2		
H20–C8–C10–C12	47.8	47.6	47.9	47.7		
H20–C8–C10–C14	151.5	151.4	151.5	151.4		
H20–C8–C10–H22	−78.1	−78.1	−78.0	−78.0		
C9–C8–C15–Cl1	162.7	162.5	162.8	162.7		
C9–C8–C15–C17	37.6	37.5	37.4	37.4		
C9–C8–C15–C18	−65.4	−65.5	−65.7	−65.7		
C10–C8–C15–Cl1	−82.6	−82.7	−82.5	−82.6		
C10–C8–C15–C17	152.4	152.3	152.1	152.1		
C10–C8–C15–C18	49.3	49.3	49.0	49.0		
H20–C8–C15–Cl1	45.4	45.2	45.1	45.2		
H20–C8–C15–C17	−79.7	−79.8	−80.2	−80.1		
H20–C8–C15–C18	177.3	177.2	176.7	176.8		
C8–C9–C11–C13	71.4	71.3	71.5	71.5		
C8–C9–C11–C14	−32.3	−32.6	−32.1	−32.3		
C8–C9–C11–H23	−162.7	−163.0	−162.6	−162.8		
C16–C9–C11–C13	−174.0	−174.2	−174.0	−174.0		
C16–C9–C11–C14	82.3	82.0	82.4	82.2		
C16–C9–C11–H23	−48.1	−48.4	−48.1	−48.3		
H21–C9–C11–C13	−47.8	−47.9	−47.9	−47.8		
H21–C9–C11–C14	−151.4	−151.7	−151.5	−151.5		
H21–C9–C11–H23	78.1	77.9	78.0	78.0		
C8–C9–C16–Cl2	−162.6	−162.7	−162.8	−162.8		
C8–C9–C16–C17	−37.6	−37.7	−37.5	−37.5		
C8–C9–C16–C19	65.5	65.3	65.6	65.6		
C11–C9–C16–Cl2	82.6	82.6	82.5	82.6		

Table 2 (*continued*)

Parameter	B3LYP[a]		Wb97xd[a]		Exp[b]	Exp[c]
	6-31G*	6-311++G**	6-31G*	6-311++G**		
C11–C9–C16–C17	−152.3	−152.4	−152.1	−152.2		
C11–C9–C16–C19	−49.3	−49.4	−49.0	−49.1		
H21–C9–C16–Cl2	−45.3	−45.5	−45.2	−45.3		
H21–C9–C16–C17	79.7	79.5	80.2	80.0		
H21–C9–C16–C19	−177.2	−177.5	−176.7	−176.9		
C8–C10–C12–O7	135.7	135.7	135.5	135.6		
C8–C10–C12–C13	73.1	73.0	73.1	73.1		
C8–C10–C12–H24	−74.0	−74.2	−73.6	−73.7		
C14–C10–C12–O7	28.6	28.7	28.3	28.4		
C14–C10–C12–C13	−34.1	−34.0	−34.2	−34.1		
C14–C10–C12–H24	178.9	178.8	179.1	179.1		
H22–C10–C12–O7	−98.8	−98.9	−99.1	−99.2		
H22–C10–C12–C13	−161.5	−161.6	−161.6	−161.7		
H22–C10–C12–H24	51.5	51.2	51.7	51.5		
C8–C10–C14–C11	−50.7	−50.8	−50.2	−50.4		
C8–C10–C14–H26	70.1	69.7	71.0	70.5		
C8–C10–C14–H27	−166.0	−166.5	−165.5	−165.9		
C12–C10–C14–C11	53.5	53.2	53.6	53.4		
C12–C10–C14–H26	174.2	173.8	174.8	174.3		
C12–C10–C14–H27	−61.9	−62.4	−61.7	−62.1		
H22–C10–C14–C11	−180.0	179.8	−179.6	−179.8		
H22–C10–C14–H26	−59.2	−59.6	−58.4	−58.9		
H22–C10–C14–H27	64.7	64.2	65.1	64.7		
C9–C11–C13–O7	−135.7	−135.8	−135.5	−135.6		
C9–C11–C13–C12	−73.0	−73.1	−73.1	−73.1		
C9–C11–C13–H25	74.0	74.2	73.6	73.7		
C14–C11–C13–O7	−28.6	−28.8	−28.3	−28.4		
C14–C11–C13–C12	34.1	33.9	34.2	34.1		
C14–C11–C13–H25	−178.9	−178.7	−179.1	−179.1		
H23–C11–C13–O7	98.8	98.8	99.2	99.2		
H23–C11–C13–C12	161.5	161.5	161.6	161.7		
H23–C11–C13–H25	−51.5	−51.2	−51.7	−51.5		
C9–C11–C14–C10	50.6	50.9	50.2	50.4		
C9–C11–C14–H26	−70.2	−69.7	−71.0	−70.4		
C9–C11–C14–H27	166.0	166.5	165.5	166.0		
C13–C11–C14–C10	−53.5	−53.2	−53.6	−53.4		
C13–C11–C14–H26	−174.3	−173.8	−174.8	−174.3		
C13–C11–C14–H27	61.9	62.4	61.7	62.1		
H23–C11–C14–C10	179.9	−179.8	179.6	179.8		
H23–C11–C14–H26	59.1	59.6	58.4	58.9		
H23–C11–C14–H27	−64.7	−64.2	−65.1	−64.7		
C10–C12–C13–C11	0.0	0.1	0.0	0.0		
C10–C12–C13–H25	−145.9	−146.1	−145.6	−145.7		
H24–C12–C13–C11	145.9	146.2	145.6	145.7		
H24–C12–C13–H25	0.0	0.0	0.0	0.0		
Cl1–C15–C17–Cl3	−64.4	−64.5	−64.5	−64.6		
Cl1–C15–C17–Cl4	59.7	59.5	59.8	59.6		
Cl1–C15–C17–C16	177.5	177.4	177.6	177.4		
C8–C15–C17–Cl3	59.2	59.2	59.3	59.3		
C8–C15–C17–Cl4	−176.7	−176.8	−176.4	−176.5		
C8–C15–C17–C16	−58.9	−58.9	−58.6	−58.7		
C18–C15–C17–Cl3	171.6	171.6	171.3	171.3		
C18–C15–C17–Cl4	−64.3	−64.4	−64.4	−64.5		
C18–C15–C17–C16	53.5	53.4	53.4	53.3		
Cl1–C15–C18–Cl5	25.3	25.6	26.0	26.4		
Cl1–C15–C18–C19	−160.3	−160.2	−160.5	−160.3		
C8–C15–C18–Cl5	−105.7	−105.7	−104.7	−104.5		
C8–C15–C18–C19	68.6	68.6	68.8	68.8		
C17–C15–C18–Cl5	149.7	149.9	150.7	150.9		
C17–C15–C18–C19	−35.9	−35.9	−35.8	−35.8		
Cl2–C16–C17–Cl3	64.4	64.5	64.5	64.6		
Cl2–C16–C17–Cl4	−59.7	−59.5	−59.8	−59.6		
Cl2–C16–C17–C15	−177.5	−177.4	−177.6	−177.4		
C9–C16–C17–Cl3	−59.2	−59.1	−59.3	−59.2		
C9–C16–C17–Cl4	176.7	176.8	176.4	176.5		
C9–C16–C17–C15	58.9	59.0	58.6	58.7		
C19–C16–C17–Cl3	−171.6	−171.5	−171.3	−171.3		
C19–C16–C17–Cl4	64.3	64.4	64.4	64.5		
C19–C16–C17–C15	−53.5	−53.4	−53.4	−53.3		
Cl2–C16–19–Cl6	−25.3	−25.5	−26.0	−26.4		
Cl2–C16–19–C18	160.3	160.1	160.5	160.3		
C9–C16–19–Cl6	105.7	105.7	104.7	104.5		
C9–C16–19–C18	−68.6	−68.6	−68.8	−68.8		

(*continued on next page*)

Table 2 (*continued*)

Parameter	B3LYP[a]		Wb97xd[a]		Exp[b]	Exp[c]
	6-31G*	6-311++G**	6-31G*	6-311++G**		
C17–C16–19–Cl6	−149.7	−149.8	−150.7	−150.9		
C17–C16–19–C18	35.9	35.8	35.8	35.8		
Cl5–C18–19–Cl6	0.0	0.0	0.0	0.0		
Cl5–C18–19–C16	174.1	174.1	173.2	173.0		
C15–C18–19–Cl6	−174.1	−174.1	−173.2	−173.0		
C15–C18–19–C16	0.0	0.0	0.0	0.0		

[a] This work.
[b] From Ref [48].
[c] From Ref. [49].

as observed in Table S2, but when the 6-311++G** basis set is used it is possible to observe higher values than the other basis set. The higher values are observed in the Cl5 and Cl6 atoms, the C atoms belonging to R1 rings and the H24 and H25 atoms. In solution, the variations in the BO values can be clearly seen when the 6-311++G++ basis set is employed. In general with this basis set, a slight decrease it is observed in the BO values corresponding to the Cl, C and H atoms.

The analysis of the molecular electrostatic potentials (MEP) values from Table S3, by using both methods and basis sets, increase in the following order, as it is expected due to the higher electronegativity of the Cl atoms than the other ones: Cl > O > C > H. The MEP values by using the 6-31G* basis set do not show differences between both methods in aqueous solution, however, when the 6-311++G* basis set is employed the values change slightly in solution. The least negative values are observed on the H24 and H25 atoms, for these reasons when we observed the mapped surface from Fig. S5 the strong blue colours are observed on these atoms indicating that these regions are electrophilic sites while on the O7 atoms are observed the strong red colours demonstrating that these regions are nucleophilic sites while the regions around the Cl atoms are slightly green and, for this reason, there are regions potentially inert.

4.3. NBO and AIM studies

The studies related to the stabilities of dieldrin in both media are very important because of their toxics properties, hence, NBO [42] and AIM [44,45] calculations were employed to analyze the donor-acceptor energy interactions and their topological properties in both media and by using the two methods and basis sets. The results presented in Table S4 show clear differences between the two studied B3LYP and WB97XD methods where the influence of both basis sets is notable especially by using the WB97XD/6-31G* method. Thus, this latter method predicts a higher total energy value (385.23 kJ/mol) for dieldrin in gas phase while in solution the WB97XD/6-311++G** method predicts a value of 311.45 kJ/mol.

The stabilities of dieldrin in both media were also performed by using the AIM calculations with the AIM 2000 program [44] because it is very important to investigate the presence of potential intra-molecular interactions and the values of their topological properties. This way, the electron density distribution, $\rho(r)$, the values of the Laplacian, $\nabla^2\rho(r)$, the eigenvalues ($\lambda 1, \lambda 2, \lambda 3$) of the Hessian matrix and the $\lambda 1/\lambda 3$ ratio were calculated in the bond critical points (BCPs) and ring critical points (RCPs) taking into account the Bader's theory [45]. This study shows two new C18···H26 and C14···O7 interactions observed only for dieldrin in gas phase with the B3LYP/6-31G* method which have characteristics of H bonds interactions because they present $\lambda 1/\lambda 3 < 1$ and $\nabla^2\rho(r) > 0$ (closed-shell interaction). Here, it is necessary to clarify that the new C18···H26 interaction is formed in gas phase from the middle of the C18–C19 bond towards the H26 atom. However, when the WB97XD method is used in the two media with both basis sets only the C18···H26 interaction it is observed and, besides, with the B3LYP/6-311++G** in solution. Then, the parameters calculated in the two BCPs C18···H26 and C14···O7 by using the two methods and both basis sets can be seen in Table S5 while in Tables S6 and S7 the properties observed in the properly RCPs of the five rings (named RCP from 1 to 5) are presented and, in those three new RCPs are observed and were named RCPN1, RCPN2 and RCPN3. In Fig. 3 the molecular graphic for dieldrin in gas phase by using the B3LYP/6-31G* method can be seen where we can observe the two C18···H26 and C14···O7 BCPs, the five RCPs of the rings and, also, those three new RCPN1, RCPN2 and RCPN3. Table S5 shows that the properties of the BCPs practically do not change neither in solution nor with the method but only, the C14···O7 interaction disappears when the basis set change from 6 to 31G* to 6-311++G** and when the medium changes from gas phase to solution. Comparisons of the topological properties in the ring critical points (RCPs) by using the two B3LYP and WB97XD methods and different basis sets for dieldrin in gas and aqueous solution phases can be seen in Figs. S6 and S7. Both figures clearly show that only the RCP5 present their properties different from the other ones with higher $\rho(r)$, $\nabla^2\rho(r)$ and $\lambda 1/\lambda 3$ values. Hence, these studies suggest: (i) the high stability of dieldrin in gas phase by using the B3LYP/6-31G* method, (ii) the dependence of the basis set, the method and the medium used to perform the calculations on the topological properties, (iii) the characteristic of the C18···H26 interaction supports that both new rings RCPN1 and RCPN2 formed can exhibit the same properties, as observed in Table S6 and S7 and, finally, (iv) the different properties observed in the RCP5 suggest that probably the R5 ring plays a very important role in the toxics properties of dieldrin.

4.4. Frontier orbitals and descriptors

Due to the toxic properties of dieldrin it is very important to evaluate their reactivities and behaviour in different media and, for this reason, the frontier orbitals were computed with both B3LYP and WB97XD methods and by using the 6-31G* and 6-311++G** basis sets. Later, in accordance to Parr and Pearson [27] the gap values were computed together with the chemical potential (μ), electronegativity (χ), global hardness (η), global softness (S) and global electrophilicity index (ω) descriptors [29–32] in order to calculate their values and predict their reactivities. These results are presented in Table S8 together with the corresponding equations used to calculate the descriptors while in Table S9 we have presented comparisons among the results obtained for dieldrin by using B3LYP/6-31G* calculations in gas phase with those reported for other chlorinated compounds such as, hexachlorobencene (C_6Cl_6) [50], 3,3′,4,4′-tetrachloroazobenzene (TCAB) [51], 3,3′,4,4′ tetrachloroazoxybenzene (TCAOB) [52] and for other toxics agents as saxitoxin (STX), ion CN^- and CO [53] by using the same level of theory. Analyzing first the gap values for dieldrin we observed that the B3LYP/6-31G* method predicted higher reactivities for dieldrin

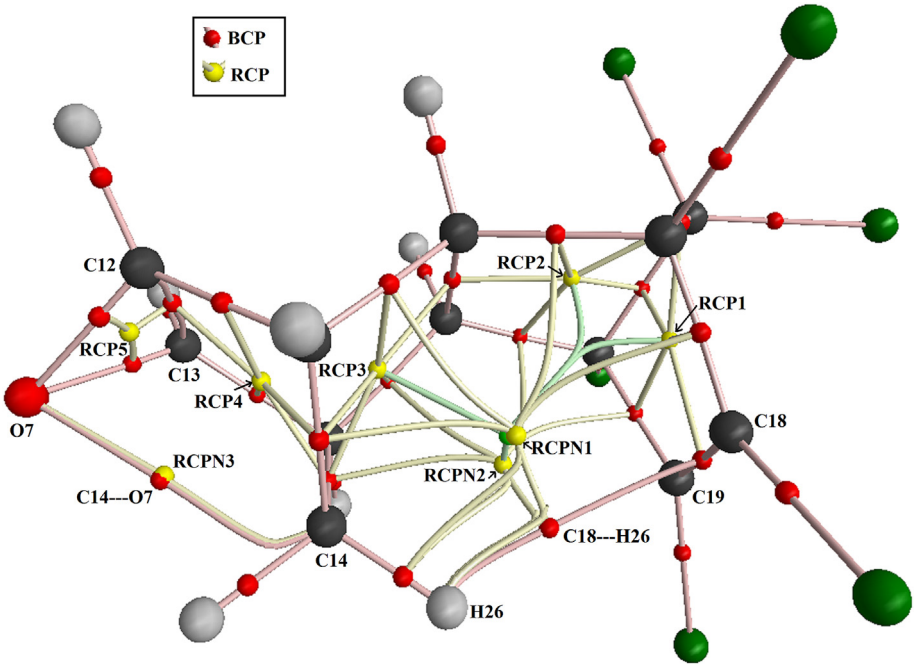

Fig. 3. Details of the molecular model for dieldrin in gas phase showing the geometry of all their bond critical points (BCPs) and ring critical points (RCPs) at the B3LYP/6-31G* level of theory.

in both media than the wb97xd/6-31G* method, showing it in solution the lower values while the reactivity increases in this medium when the B3LYP/6-311++G** method is used. Hence, the election of the method is very important in dieldrin to explain these properties. The descriptors are also influenced by the method, hence, the higher ω and E values are observed for dieldrin in solution with the wb97xd/6-311++G** method while the low values are observed for dieldrin in gas phase by using the B3LYP/6-311++G** level of theory. The comparisons of these properties for dieldrin with other of species toxics can better be seen from Fig. S8. Thus, the frontier orbitals of dieldrin show practically the same behaviour than hexachlorobencene [50] while these orbitals for 3,3′,4,4′-tetrachloroazobenzene (TCAB) [51] have the same behaviour than 3,3′,4,4′ tetrachloroazoxybenzene (TCAOB) [52], as it is expected because both have similar structures but, the saxitoxin (STX), ion CN^- and CO [53] species show behaviours completely different from the other species. Table S9 shows clearly that the reactivity increases in the following order: CO < STX < dieldrin < C_6Cl_6 <TCAB < TCAOB < CN^-. Evidently, the presence of five rings and six Cl atoms decreases the reactivity of dieldrin, as compared with hexachlorobencene [50] while TCAB, TCAOB and CN^- are the most reactive species. When the descriptors are compared, from Fig. S8, we observed that χ, η and *S* do not change and only changes in μ, ω and *E* are observed. Hence, the high global electrophilicity index observed for CN^- could probably explain in part their high toxicity.

4.5. Vibrational study

The theoretical dieldrin structures modelled with both B3LYP and WB97XD methods and the two 6-31G* and 6-311++G** basis sets were optimized with C_1 symmetries and, due to the presence of 27 atoms in their structure, 75 vibration normal modes are expected. In Fig. 4 the experimental IR spectrum of dieldrin in the solid state can be seen compared with the corresponding predicted in gas phase by using both methods while in Fig. 5 the experimental Raman spectrum and their comparisons is presented with the theoretical ones. Both figures show a satisfactory correlation among the experimental and theoretical spectra in their intensities, positions and forms of the bands. In the 3500-2000 cm^{-1} and 1800-500 cm^{-1} wavenumbers regions it is observed that in both predicted IR and Raman spectra by using the two methods the bands are slight shifted in relation to the observed in the experimental ones. These differences observed in the higher wavenumbers region can be attributed in part to the calculations because they were performed considering harmonic frequencies where the anharmonicity due to the H atoms was no considered. On the other hand, the calculations were performed in gas phase where the molecules move freely while in the solid state the forces due to the crystalline packing are important.

In particular, the activities predicted by the calculations for the Raman spectra with both methods were corrected to intensities by know equations [54,55] and, for this reasons, their comparisons with the experimental one show a very good concordance. The harmonic SQMFF approach [25] and the Molvib program [26] were used to perform the complete vibrational assignments taking into account their internal coordinates and the potential energy distribution (PED) contributions ≥ 10%. Besides, the scale factors used were those reported by Rauhut and Pulay [25] by using the B3LYP method. Here, the internal normal coordinates as redundant as a consequence of the different fused rings that were removed, in a way that was similar to the performed for tropane alkaloids [36,37,46]. The observed and calculated wavenumbers and assignments for dieldrin in gas phase by using B3LYP/6-31G* and WB97XD/6-31G* levels of theory can be seen in Table 3. Note that there are notable differences in the assignments between both methods because many modes are predicted coupled with other ones and at different wavenumbers, as indicated in Table 3. Besides, it is necessary to clarify that in this work the harmonic force fields were performed with both methods and basis sets. Some important assignments were discussed below only for dieldrin in gas phase by using the B3LYP/6-31G* method.

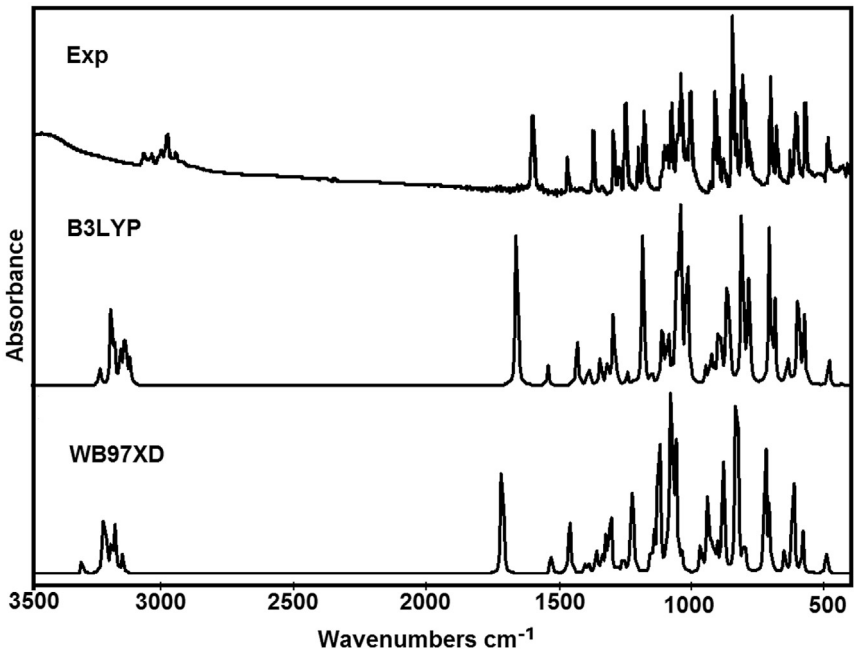

Fig. 4. Comparisons between the experimental FTIR spectra of dieldrin with the corresponding predicted in the gas phase at B3LYP/6-31G* and WB97XD/6-31G* levels of theory.

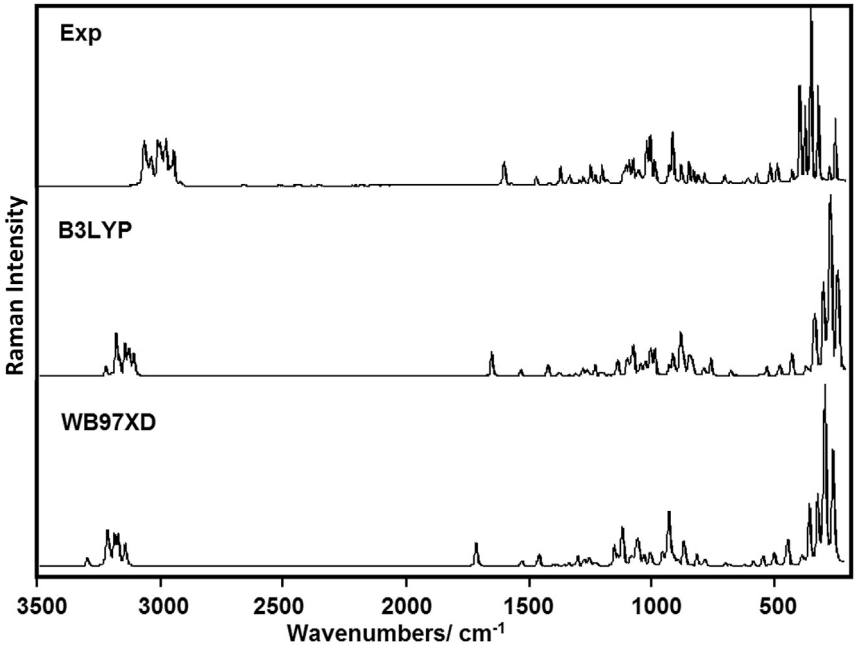

Fig. 5. Comparisons between the experimental FTRaman spectra of dieldrin with the corresponding predicted in the gas phase at B3LYP/6-31G* and WB97XD/6-31G* levels of theory.

4.5.1. Band assignments

4.5.1.1. CH modes. In dieldrin, the C–H stretching modes are formed by aliphatic C atoms with sp^3 hybridization, very different from TCAB [51] and TCAOB [52] where the vibration CH modes belong to aromatic C atoms with sp^2 hybridization. Hence, for dieldrin the CH stretching are expected, rocking and CCC and CCO deformation modes depending from the involved H atoms. Thus, the CH stretching, rocking and CCC or CCO deformation modes are predicted by SQM/B3LYP/6-31G* calculations respectively between 3053/2979, 1387/993 and 1056/477 cm^{-1}. Therefore, the IR and Raman bands, observed in the different 3063/2973, 1389/1004 and 1051/487 cm^{-1} regions, are assigned to those vibration modes, as it is detailed in Table 3.

4.5.1.2. CH_2 modes. Dieldrin presents a CH2 group and, for this reason, six vibration modes related to this group are expected. Hence, the antisymmetrical stretching mode is predicted at 3092 cm−1 while the corresponding symmetrical mode at 3018 cm−1.Thus the IR bands at 3063 and 3032 cm−1 are clearly assigned to both stretching modes while the IR bands at 1468, 1334,

Table 3
Observed and calculated wavenumbers (cm^{-1}) and assignment for the Dieldrin in gas phase by using the B3LYP and WB97XD methods and the 6-31G* basis set.

Experimental[a]		B3LYP			wb97xd		
IR Solid	Raman Solid	IR Calc.	SQM	Assignment	IR Cal.	SQM	Assignment
		3226	3092	ν_aCH_2	3294	3156	ν_aCH_2
3063w	3062 m	3184	3053	$\nu_sC{-}H$(C12,C13)	3215	3082	$\nu_sC{-}H$(C12,C13)
3050w	3062 m	3173	3042	$\nu_aC{-}H$(C12,C13)	3203	3071	$\nu_aC{-}H$(C12,C13)
3032w	3034 m	3148	3018	ν_sCH_2	3183	3051	ν_sCH_2
2997w	3008 m	3133	3003	νC10−H22	3170	3039	νC10−H22
2997w	2998 m	3132	3003	νC11−H23	3168	3037	νC11−H23
2981w	2982 m	3115	2986	$\nu_sC{-}H$(C8,C9)	3142	3012	$\nu_sC{-}H$(C8,C9)
2973w	2975 m	3108	2979	$\nu_aC{-}H$(C8,C9)	3135	3005	$\nu_aC{-}H$(C8,C9)
1597 m	1599 m	1657	1594	νC18 = C19	1713	1647	νC18 = C19
1468w	1469w	1539	1471	δCH_2	1529	1462	δCH_2
1389vw		1431	1387	ρC13−H25	1459	1411	ρC13−H25
1371 m	1371w	1389	1354	ρ′C9−H21	1402	1365	ρ′C8−H20
1341sh	1340sh	1382	1343	ρ′C8−H20	1388	1350	ρ′C9−H21
1334w	1332w	1343	1315	$wagCH_2$	1357	1326	ρ′C12−H24
1298s	1295vwv	1319	1286	ρ′C12−H24	1337	1300	ρC10−H22
1276 m	1278vw	1315	1282	ρC11−H23	1322	1293	$wagCH_2$
1270 m		1296	1263	ρC8−H20	1306	1274	ρC8−H20
1248 m	1248w	1288	1251	ρ′C11−H23, ρ′C10−H22	1303	1265	ρ′C10−H22,ρ′C11−H23
1229vw	1230ww	1271	1238	ρC10−H22	1277	1244	ρC11−H23
1200mw	1201w	1241	1204	ρ′C12−H24, νC12−C13	1256	1221	ρ′C12−H24
1178 m	1181vw	1216	1180	ρC8−H20, ρC10−H22	1238	1202	νC8−C10
1178 m	1181vw	1207	1179	ρC9−H21	1229	1198	ρC9−H21,νC9−C11
1132vw	1147vvw	1184	1150	νC19−C16	1222	1186	νC18−C15
1115w	1115w	1150	1123	ρCH_2	1155	1127	ρCH_2
1103w	1103w	1113	1084	ρ′C13−H25	1142	1103	νC19−Cl6
1091w	1090 m	1108	1072	βR_2(A2)	1126	1102	νC16−C19
1075 m	1075 m	1094	1069	νC18−C15	1125	1096	ρ′C13−H25
1051 m	1052w	1087	1056	δC−C−C	1120	1087	βR_1(A2),
1040s	1019 m	1059	1016	νC8−C15	1088	1049	νC8−C15
1019w	1005 m	1045	1015	νC9−C11	1076	1042	νC9−C16
1004s		1039	993	ρC12−H24	1067	1033	νC15−C17
988w	988 m	1019	985	βR_1(A2), τR_2(A1)	1057	1011	ρC12−H24
988w	982sh	1016	984	νC9−C16	1037	1005	ρ′C11−H23
956sh	969sh	1002	962	τR_2(A3)	1012	977	τR_2(A3)
930w	928w	946	919	βR_2(A4), νC11−C14	965	932	βR_2(A4),
911s	915 m	942	902	βR_1(A2), τ_wCH_2	964	927	νC8−C9, νC10−C12
899 m		930	897	νC10−C14	955	917	τ_wCH_2
880w	881w	922	888	νC11−C13,νC10−C12, νC12−O7	943	909	νC10−C14
873w	870sh	901	864	τR_2(A2), τ_wCCl_2	937	896	τR_2(A29)
863sh		891	857	νC8−C9	921	882	νC8−C9
846 vs	847 m	870	840	νC15−C17, νC16−C7	905	873	νC15−C17
830 m	830w	864	834	νC12−C13	881	851	νC12−C13
809s	810w	855	828	νC13−O7	877	850	νC12−O7 νC11−C13
800 m	801vw	810	792	βR_1(A4)	831	806	βR_2(A2)
784 m	785w	809	789	βR_2(A2)	826	803	βR_1(A4)
777sh	763vvw	785	765	νC11−C14	802	786	ν_aCCl_2
769sh	763vvw	784	760	ν_aCCl_2	797	779	νC11−C14
703s	704w	706	683	ν_sCCl_2, δC−C−C	722	698	δC−C−C
681 m		687	672	$wagCCl_2$, τR_1(A1)	706	690	$wagCCl_2$
629w	630vw	640	628	βR_2(A4), βR_2(A3)	651	640	βR_2(A3)
607 m	607vw	628	618	$\gamma_aC18{-}Cl5$, τR_1(A1)	645	635	γ_aC18-Cl5
572 m	572w	599	578	τR_2(A3), ν_aCCl_2	618	598	τR_2(A1)
550vw	540vvw	575	553	τR_2(A4)	582	559	τR_2(A4)
519vw	517 m	528	519	$\gamma_aC18{-}Cl5$	542	533	γ_aC18-Cl5
487 m	488w	484	477	δC−C−O	493	483	δC−C−O
415w	428w	432	422	τR_1(A4)	440	430	τR_1(A3),
398w	396s	402	388	$\gamma_sC18{-}Cl5$, τR_2(A3)	413	399	ν_sCCl_2
375 vs	376s	370	357	ν_sCCl_2, νC15−Cl1	384	371	νC15−Cl1
	351vs	353	342	βR_2(A1), νC18−Cl5,νC19−Cl6	362	351	βR_2(A1),νC18−Cl5
	322s	345	331	νC16−Cl2	358	344	νC16−Cl2
	310vvw	319	310	τR_1(A4), βR_2(A2)	329	317	τR_1(A4)
	300vvw	318	305	ν_aCCl_2, τR_2(A2)	325	314	τR_2(A2)
	275w	271	258	τ_wCCl_2	275	262	τ_wCCl_2
	253s	250	246	δCCl_2	257	253	δCCl_2
	213vw	187	182	ρC18−Cl5	192	188	ρC18-Cl5
	187vvw	184	181	ρC16−Cl2, ρC15−Cl1	189	185	ρ′C15−Cl1
	170vvw	173	171	ρC19−Cl6	177	175	ρC19−Cl6
	165vvw	165	163	$wagCCl_2$, ρ′C16−Cl2	170	167	ρ′C16−Cl2
	150vvw	155	152	ρ′C15−Cl1	160	158	ρC16−Cl2
	140vvw	142	140	ρCCl_2	146	145	ρC15−Cl1
	122vvw	126	123	ρCCl_2, τR_1(A3)	128	126	ρCCl_2
	110vvw	111	106	τR_1(A3), τR_1(A2)	114	109	τR_2(A1)
	106vvw	109	105	τR_2(A2)	109	107	τR_1(A2)

(*continued on next page*)

Table 3 (*continued*)

Experimental[a]		B3LYP			wb97xd		
IR Solid	Raman Solid	IR Calc.	SQM	Assignment	IR Cal.	SQM	Assignment
		90	88	$\tau R_1(A1)$	95	93	$\tau R_1(A1)$
		80	78	$\gamma_s C18{-}Cl5$, $\tau R_2(A1)$	87	85	$\gamma_s C18{-}Cl5$

Abbreviations ν, stretching; β, deformation in the plane; γ, deformation out of plane; wag, wagging; τ, torsion; β_R, deformation ring τ_R, torsion ring; ρ, rocking; τw, twisting; δ, deformation; a, antisymmetric; s, symmetric; A1, Ring 1; A2, Ring 2; A3, Ring 3; A4, Ring 4; A5, Ring 5.

[a] This work.

1115 and 911 cm−1 are associated to the CH2 deformation, rocking, wagging and twisting modes, respectively because they are predicted by SQM/B3LYP/6-31G* calculations in these regions.

4.5.1.3. CCl modes. Dieldrin has six Cl atoms, of which two, belong to a CeCl2 group, two belong to C atoms with sp2 hybridization and, the other two CeCl groups belong to C atoms with sp3 hybridization. Obviously, all these modes are expected at different wavenumbers. Thus, the antisymmetrical CeCl2 stretching mode is predicted at 760 cm−1 while the corresponding symmetrical mode is predicted coupled with a CeCl stretching mode at 683/357 cm−1, hence, they can be easily assigned in these regions. The expected CeCl2 twisting, wagging, deformation, and rocking modes are predicted at 864/258, 683/163, 246 and 140/123 cm−1 and, for this reason, the observed Raman bands in theses regions can be clearly assigned to those vibration modes. For the CeCl groups belong to C atoms with sp2 hybridization are expected the stretching, rocking and out-of-plane deformation modes, as in the aromatic CeH groups. In aromatic compounds, as in TCAB, the CeCl stretching modes were assigned between 606 and 442 cm−1 [51] while in the Trans isomers of TCAOB [52] these modes are assigned between 795 and 372 cm−1 while for the Cis forms they are assigned between 782 and 401 cm−1. Hence, the C18eCl5 and C19eCl6 stretching modes are assigned at 1132 and 1075 cm−1 because they are predicted at 1150 and 1069 cm−1, respectively although these modes are predicted coupled at 342 cm−1. The rocking modes are predicted at lower wavenumbers than the out-of-plane modes and, hence, they can be associated to the very weak Raman bands at 213 and 170 cm−1 while the out-of-plane modes are predicted in phase between them and in the 618/519/388/78 cm−1 regions coupled with other modes. The other modes related to the two CeCl groups belong to C atoms with sp3 hybridization are the stretching and rocking modes, therefore, the strong Raman bands at 376, 351 and 322 cm−1 are associated to the vibration CeCl stretching modes because they are predicted by the SQM calculations in these regions. The rocking modes of these groups are expected in the 182/152 cm−1 region, as observed in Table 3.

4.5.1.4. Skeletal modes. Two CeO stretching modes are expected for dieldrin which belongs to the ring R5 (C12eO7 and C13eO7). Both are predicted at 888 and 828 cm−1, thus, the weak and strong IR bands at 880 and 809 cm−1 are assigned to those two stretching modes. The C18 = C19 stretching modes are predicted by the SQM/B3LYP/6-31G* calculations at 1594 cm−1; hence, it is assigned at 1597 cm−1. On the other hand, the CeC stretching modes were predicted between 1204 and 765 cm−1and, for this reason, they are assigned as predicted by the SQM calculations and as observed in Table 3. The expected deformation and torsion ring modes for the five rings are predicted in approximately the same regions reported for other fused rings [36,37,46] and, as a consequence they are clearly assigned in those regions. The assignments of the remaining skeletal modes expected for dieldrin can be seen in Table 3.

5. Force fields

For dieldrin in gas and aqueous solution phases we have calculated the harmonic forces constants from their corresponding harmonic force fields computed employing the SQM procedure [25] and the Molvib program [26] with the B3LYP and WB97XD methods and the two 6-31G* and 6-311++G** basis sets. Thus, the results are summarized in Table 4 compared with those reported for TCAB and TCAOB [51,52]. Here, we clarify that the *f(νC-Cl)* forces constants are different from the *f(νC-Cl$_2$)* ones because the former are related to the C—Cl bonds and the second ones specifically to the C—Cl$_2$ group.

Regarding first the calculated values by using the hybrid B3LYP/6-31G* method in different media we observed that the values for the *f(νCH$_2$)* and *f(νC-H)* forces constants slightly increase in solution while the values corresponding to *f(νC-O)*, *f(νC-Cl)* and *f(νC-Cl$_2$)* decrease in that medium. These diminishing in solution probably are related to the hydration of dieldrin with the water molecules. When the forces constants are compared at the same level of theory with the other basis set we observed a significant decrease in the values in both media. Analyzing the obtained values by using the WB97XD level of theory, the values by using the 6-31G* basis set are higher than those calculated by using the B3LYP method and the same variations are observed in the forces constants values. Hence, in solution the *f(νCH$_2$)* and *f(νC-H)* forces constants slightly increase while the *f(νC-O)*, *f(νC-Cl)* and *f(νC-Cl$_2$)* decrease in this medium. When they increase, the size of the basis set all force constant values decreases by using the WB97XD method. A very important result is that for a same basis set the *f(νC-C)* force constants remaining practically constant which implies that the C—C bonds do not change in solution, as it is expected because these bonds are not hydrated due to that they belong to the different rings. On the other hand, when the values are compared with those reported for TCAB and TCAOB [51,52] the difference among the *f(νC-H)* and *f(νC-C)* forces constants is notable because these two species with rings are planar and where the C—H bonds present the C atoms in sp^2 hybridization. On the contrary, in dieldrin the ring are not planar and the C atoms belong to the rings have sp^3 hybridization. In particular, the *f(νC-Cl)* forces constants by using the B3LYP/6-31G* method for dieldrin are practically similar to those calculated for TCAB and TCAOB [51,52] because in dieldrin two C—Cl bonds have their C atoms in sp^2 hybridization.

6. NMR study

In this study, the Gauge-Independent Atomic Orbital (GIAO) method [56] using tetramethylsilane (TMS) as reference was employed in order to compute the ^{1}H and ^{13}C chemical shifts for dieldrin. The experimental available ^{1}H and ^{13}C NMR spectra of dieldrin in $CDCl_3$ were taken from Refs. [57,58]. On the other hand, in Table S10 the predicted ^{1}H and ^{13}C NMR chemical shifts are summarized by using the GIAO method [56] with both B3LYP and WB97XD methods and the two basis sets in ethanol and $CHCl_3$ solution. The comparisons between the calculated values with the corresponding experimental ones were performed by using the

Table 4
Comparison of calculated harmonic scaled internal force constants for dieldrin in gas and aqueous solution phases by using two methods an.

Force constants	B3LYP[a]				Wb97xd[a]				B3LYP	
									6-31G*	
	6-31G*		6311++G**		6-31G*		6-311++G**		TCAB[b]	TCAOB[c]
	Gas	PCM	Gas	PCM	Gas	PCM	Gas	PCM	*Trans I*	*Trans II*
f(νCH$_2$)	5.04	5.08	4.98	5.02	5.16	5.18	5.08	5.07		
f(νC–H)	4.96	5.00	4.89	4.93	5.08	5.11	5.00	5.02	5.261	5.344
f(νC–O)	3.94	3.68	3.78	3.46	4.36	4.08	4.21	3.93		
f(νC–C)	4.02	4.02	3.96	3.97	4.28	4.29	4.25	4.24	6.447	6.476
f(νC–Cl)	3.42	3.35	3.36	3.31	3.72	3.66	3.70	3.61	3.430	3.454
f(νC–Cl$_2$)	2.77	2.70	2.74	2.66	3.13	3.06	3.08	3.02		

Units are mdyn Å^{-1} for stretching and stretching/stretching interaction.
[a] This work.
[b] From Ref [51].
[c] From Ref [52].

RMSD values. Thus, analyzing the calculated values we observed that for the ^{1}H nucleus there is a very good concordance with values between 0.7 and 0.3 ppm while for the ^{13}C nucleus the rmsd values increase between 12.9 and 5.3 ppm because the values are overestimated in relation to the experimental ones, as observed in compound with rings [31,59]. Here, the RMSD values show a better correlation for both H and C nucleus by using the WB97XD/6-311++G** calculations. Here, probably the differences observed among the calculated and experimental the ^{1}H and ^{13}C chemical shifts values could be attributed in part to the calculations because they were performed for dieldrin in ethanol and $CHCl_3$ solution instead $CDCl_3$.

7. Ultraviolet–visible spectrum

The electronic spectrum of dieldrin recorded in $CHCl_3$ solution was compared with the corresponding predicted in the same medium by using Time-dependent DFT calculations (TD-DFT) at the B3LYP/6-31G* and 6-311++G** levels of theory with the Gaussian 09 program [41]. These comparisons can be observed in Fig. 6. The experimental spectrum shows a very intense band at 249 nm and, between 200 and 249 nm, a total of seven bands of approximately the same intensities located at 231, 224, 219, 218, 213, 209 and 204 nm are observed being the most weak band that observed at 219 nm. On the other hand, the theoretical spectrum by using the B3LYP/6-31G* method predicted in total four bands where three of them are located between 140 and 200 nm which are, a very strong band at 144 nm and the other one weak at 159 and 189 nm, respectively. Then, between 200 and 300 nm a band of medium intensity at 217 nm is predicted. Obviously, the experimental UV spectra was recorded from 200 to 500 nm and, for this reason, there are not bands observed in the 100–200 nm region. In the theoretical spectrum predicted by using the B3LYP/6-311++G** level of theory only three bands of strong, weak and medium intensities are observed at 160, 192 and 223 nm, respectively. Dieldrin presents a C=C double bond in their structure, hence, the bands calculated at lower wavelengths can be easily assigned to $n\rightarrow\pi^*$ transitions due to the lone pairs of the six Cl atoms, as predicted by NBO calculations (Table S4), while the band observed in the experimental spectrum at 249 nm could be attributed to the $\pi\rightarrow\pi^*$ transitions, as reported for compounds with C=C bonds [31,59–61].

8. Conclusions

Here, dieldrin in the solid phase has been characterized by using the FTIR and Raman spectroscopies and in ethanol solution by using UV–Visible spectroscopy. The molecular structures in gas phase and in aqueous solution were theoretically studied by using the hybrids B3LYP and WB97XD methods with the two 6-31G* and 6-311++G** basis sets. The results show that the B3LYP/6-311++G** method generates the most stable structures for dieldrin while all the calculations have demonstrated certain dependence of the volume and dipole moment values with the method, size of the basis set and, with the studied media. In particular, the lower solvation energy for dieldrin (−32.94 kJ/mol) is observed for the higher contraction volume (−2.4 Å^3) by using the B3LYP/6-31G* method. The studies of the MK and NPA charges have showed that both methods and set basis have notable effects on those two charges. The NBO studies suggest a high stability of dieldrin in gas phase by using the WB97XD/6-31G* method due to the $n\rightarrow\pi^*$ and $n^*\rightarrow\pi^*$ interactions while the AIM analyses support the high

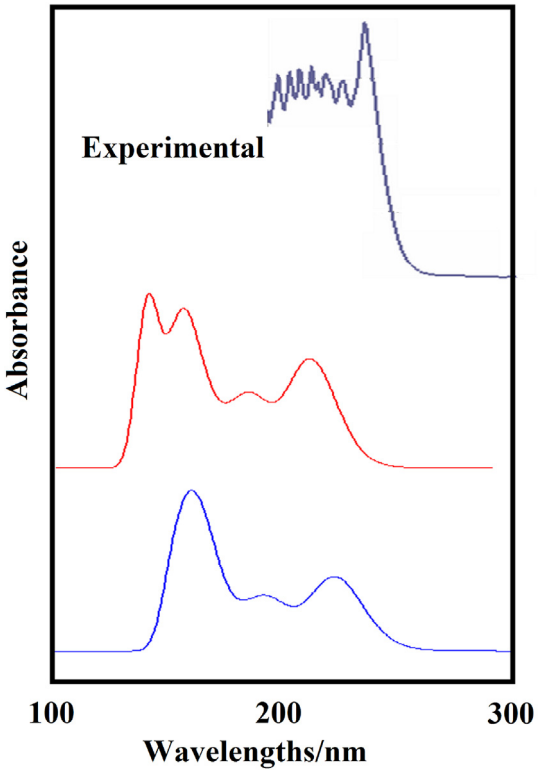

Fig. 6. Comparisons between the experimental ultraviolet–visible spectra of dieldrin in $CHCl_3$ solution (Top) with the corresponding predicted in the same solution at B3LYP/6-31G* (medium) and 6-311++G** levels (Bottom) of theory.

stability of dieldrin in that medium attributed to the C18···H26 and C14···O7 contacts. Besides, the different topological properties observed in the R5 ring suggest that it probably plays a very important role in the toxics properties of dieldrin. The frontier orbitals show that when dieldrin is compared with other toxics substances the reactivity increases in the following order: CO < STX < dieldrin < C_6Cl_6 <TCAB < TCAOB < CN^- where evidently, the presence of five rings and six Cl atoms decrease the reactivity of dieldrin, as compared with hexachlorobencene. Moreover, the WB97XD method and the two basis sets predicted for dieldrin low reactivities, higher nucleophilicity anf low electrophilicity in both media.

All the bands observed in the infrared and Raman spectra were completely assigned to the 75 vibration normal modes and their harmonic force fields and harmonic force constants for firs time are reported for dieldrin.

The comparisons among the experimental FTIR, FT-Raman, UV–Visible and ^1H and ^{13}C NMR spectra and their corresponding theoretical ones present a very good concordance.

Acknowledgements

This work was supported with grants from CIUNT Project Nº 26/D207 (Consejo de Investigaciones, Universidad Nacional de Tucumán). The authors would like to thank Prof. Tom Sundius for his permission to use MOLVIB.

Appendix A. Supplementary data

Supplementary data related to this article can be found at https://doi.org/10.1016/j.molstruc.2017.10.065.

References

[1] M. Hayashi, F. Matsumura, Insecticide mode of action. Effect of dieldrin on ion movement in the nervous system of Periplaneta americana and Blattella germanica corckroaches, J. Agric. Food Chem. 15 (4) (1967) 622–627.
[2] B. Kimland, A.J. Aasen, C.R. Enzell, Neutral volatile constituents of Greek tobacco, Acta Chem. Scand. 26 (3) (1972) 1281–1284.
[3] M.K. Baldwin, R.A. Davis, D.T. Burns, Structural studies and photochemical rearrangement of an animal metabolite of HEOD, the active component of dieldrin, Pest. Sci. 4(29 (1973) 227–237.
[4] M.M. Gomez-Taylor, D. Kuehl, P.R. Griffiths, Vibrational spectrometry of pesticides and related materials on thin layer chromatography adsorbents, Appl. Spectrosc. 30 (4) (1976).
[5] G.R. Fox, The Toxicological Significance and Etiology of the Dieldrin (HEOD)-induced Hyperglycemic Response in the Immature and Adult Rat, Electronic Theses and Dissertations, University of Windsor, 1983. Paper 4320.
[6] I. Scheunert, in: P. Bourdeau, J.A. Haines, W. Klein, C. R (Eds.), Chapter 5.4, Fate and Effects of Aldrin/Dieldrin in TerrestrialEcosystems in Hot Climates, Ecotoxicology and Climate, Published by John Wiley & Sons Ltd, 1989.
[7] T. Visser, M.J. Vredenbregt, Cryotrapping gas chromatography-Fourier transform infrared spectrometry in environmental analysis: a pilot study, Vib. Spectrosc. 1 (1990) 205–210.
[8] R. McMillin, L.C. Miner, L. Hurst, Abbreviated microwave extraction of pesticides and PCBs in soil, Spectroscopy 13 (1996/1997) 41–50.
[9] A. Nestorovska-Krsteska, Z. Zdravkovski, Theoretical study of the diastereofacial isomers of aldrin and dieldrin, Int. J. Mol. Sci. 7 (2006) 35–46.
[10] C.J. Martyniuk, K.J. Kroll, N.J. Doperalski, D.S. Barber, N.D. Denslow, Genomic, Proteomic Responses, To environmentally relevant exposures to dieldrin: indicators of neurodegeneration? Toxicol. Sci. 117 (1) (2010) 190–199.
[11] R. Reigart, Chapter 21, Chronic Effects, Environmental Protection Agency, 2013, pp. 212–238.
[12] T. Katagi, Soil column leaching of pesticides, in: D.M. Whitacre (Ed.), Reviews of Environmental Contamination and Toxicology, Springer Science Reviews of Environmental Contamination and Toxicology 221, 2013.
[13] E.M.G. Allen, V.R. Florang, L.L. Davenport, Y. Jinsma, J.A. Doorn, Cellular localization of dieldrin and structure-activity relationship of dieldrin analogues in dopaminergic cells, Chem. Res. Toxicol. 26 (7) (2013) 1043–1054.
[14] J. Kubacková, Detection of Organochlorine Pesticides by Surface-enhanced Raman Scattering on Dithiol-functionalized Plasmon Nanoparticles, Doctoral Thesis, Instituto de Estructura de la Materia Consejo Superior de Investigaciones Científicas, Madrid, España, 2014.
[15] E. Alejo-Molina, A.R. Vilchis-Néstor, D. Muñoz-Rodríguez, C. Carrera-Figueiras, Synthesis and characterization of TiO_2 modified with polystyrene and poly(3-chloro-2-hydroxypropyl methacrylate) as adsorbents for the solid phase extraction of organophosphorus pesticides, J. Chem. (2016), 1289592, 11 pages, Hindawi Publishing Corporation.
[16] J. Kubackova, G. Fabriciova, P. Miskovsky, D. Jancura, S. Sanchez-Cortes, Sensitive SERS detection of organochlorine pesticides by alkyl dithiol-functionalized metal nanoparticles induced plasmonic hot spots, Anal. Chem. 87 (1) (2015) 663–669.
[17] S. Feng, F. Ma, R. Liu, S. Li, X. Li, Y. Jin, G. Fu, X. Yue, Highly efficient removal of trace level dieldrin from water resource utilizing a cerasomal strategy, J. Mater. Chem. A 4 (2016) 10263–10273.
[18] R. Strong, F.L. Martin, K.C. Jones, R.F. Shore, C.J. Halsall, Subtle effects of environmental stress observed in the early life stages of the Common frog, Rana Temp. Sci. Rep. 7 (2017) 1–13, https://doi.org/10.1038/srep44438, 44438.
[19] A.D. Becke, Density-functional exchange-energy approximation with correct asymptotic behavior, Phys. Rev. A38 (1988) 3098–3100.
[20] C. Lee, W. Yang, R.G. Parr, Development of the Colle-Salvetti correlation-energy formula into a functional of the electron density, Phys. Rev. B 37 (1988) 785–789.
[21] J.-D. Chai, M. Head-Gordon, Long-range corrected hybrid density functionals with damped atom-atom dispersion corrections, Phys. Chem. Chem. Phys. 10 (2008) 6615–6620.
[22] S. Miertus, E. Scrocco, J. Tomasi, Electrostatic interaction of a solute with a continuum, Chem. Phys. 55 (1981) 117–129.
[23] J. Tomasi, J. Persico, Molecular interactions in solution: an overview of methods based on continous distributions of the solvent, Chem. Rev. 94 (1994) 2027–2094.
[24] A.V. Marenich, C.J. Cramer, D.G. Truhlar, Universal solvation model based on solute electron density and a continuum model of the solvent defined by the bulk dielectric constant and atomic surface tensions, J. Phys. Chem. B 113 (2009) 6378–6396.
[25] a) G. Rauhut, P. Pulay, J. Phys. Chem. 99 (1995) 3093–3099;
b) G. Rauhut, P. Pulay, Correction, J. Phys. Chem. 99 (1995) 14572.
[26] T. Sundius, Scaling of ab initio force fields by MOLVIB, Vib. Spectrosc. 29 (2002) 89–95.
[27] R.G. Parr, R.G. Pearson, Absolute hardness: companion parameter to absolute electronegativity, J. Am. Chem. Soc. 105 (1983) 7512–7516.
[28] J.-L. Brédas, Mind the gap!, Mater. Horizons 1 (2014) 17–19.
[29] M.V. Castillo, R.A. Rudyk, L. Davies, S.A. Brandan, Analysis of the structure and the FT-IR and Raman spectra of 2-(4-nitrophenyl)-4H-3,1-benzoxazin-4-one. Comparisons with the chlorinated and methylated derivatives, J. Mol. Struct. 1140 (2017) 2–11.
[30] D. Romani, S.A. Brandán, M.J. Márquez, M.B. Márquez, Structural, topological and vibrational properties of an isothiazole derivatives series with antiviral activities, J. Mol. Struct. 1100 (2015) 279–289.
[31] F. Chain, M.A. Iramain, A. Grau, C.A.N. Catalán, S.A. Brandán, Evaluation of the structural, electronic, topological and vibrational properties of *N*-(3,4-dimethoxybenzyl)-hexadecanamide isolated from Maca (*Lepidium meyenii*) using different spectroscopic techniques, J. Mol. Struct. 1119 (2016) 25–38.
[32] E. Romano, L. Davies, S.A. Brandán, Structural properties and FTIR-Raman spectra of the anti-hypertensive clonidine hydrochloride agent and their dimeric species, J. Mol. Struct. 1133 (2017) 226–235.
[33] M.B. Márquez, S.A. Brandán, A structural and vibrational investigation on the antiviral deoxyribonucleoside thymidine agent in gas and aqueous solution phases, Int. J. Quantum Chem. 114 (2014) 209–221.
[34] P.G. Cataldo, M.V. Castillo, S.A. Brandán, Quantum mechanical modeling of fluoromethylated-pyrrol derivatives a study on their reactivities, structures and vibrational properties, J. Phys. Chem. Biophys. 4 (1) (2014) 4–9.
[35] M.J. Márquez, M.B. Márquez, P.G. Cataldo, S.A. Brandán, A comparative study on the structural and vibrational properties of two potential antimicrobial and anticancer cyanopyridine derivatives, Open J. Synth. Theory Appl. 4 (2015) 1–19.
[36] R. Rudyk, S.A. Brandán, Vibrational assignment of alkaloid tropane hydrochloride by using their infrared spectrum, internal coordinates and the SQM procedure, Paripex A Indian J. Res. 6 (8) (2017) 616–623.
[37] D. Romani, S.A. Brandán, Vibrational analyses of alkaloid cocaine as free base, cationic and hydrochloride species based on their internal coordinates and force fields, Paripex A Indian J. Res. 6 (9) (2017) 587–602.
[38] N. Issaoui, H. Ghalla, S.A. Brandán, F. Bardak, H.T. Flakus, A. Atac, B. Oujia, Experimental FTIR and FT-Raman and theoretical studies on the molecular structures of monomer and dimer of 3-thiopheneacrylic acid, J. Mol. Struct. 1135 (2017) 209–221.
[39] Dieldrin structure, https://pubchem.ncbi.nlm.nih.gov/compound/dieldrin.
[40] A.B. Nielsen, A.J. Holder, Gauss View 3.0, User's Reference, GAUSSIAN Inc., Pittsburgh, PA, 2000–2003.
[41] M.J. Frisch, G. W. Trucks, H.B. Schlegel, G.E. Scuseria, M.A. Robb, J.R. Cheeseman, G. Scalmani, V. Barone, B. Mennucci, G.A. Petersson, H. Nakatsuji, M. Caricato, X. Li, H.P. Hratchian, A.F. Izmaylov, J. Bloino, G. Zheng, J.L. Sonnenberg, M. Hada, M. Ehara, K. Toyota, R. Fukuda, J. Hasegawa, M. Ishida, T. Nakajima, Y. Honda, O. Kitao, H. Nakai, T. Vreven, J.A. Montgomery, Jr., J.E. Peralta, F. Ogliaro, M. Bearpark, J.J. Heyd, E. Brothers, K. N. Kudin, V.N. Staroverov, R. Kobayashi, J. Normand, K. Raghavachari, A. Rendell, J.C. Burant, S.S. Iyengar, J. Tomasi, M. Cossi, N. Rega, J.M. Millam, M. Klene, J.E. Knox, J.B. Cross, V. Bakken, C. Adamo, J. Jaramillo, R. Gomperts, R.E. Stratmann, O. Yazyev, A.J.

Austin, R. Cammi, C. Pomelli, J.W. Ochterski, R.L. Martin, K. Morokuma, V.G. Zakrzewski, G.A. Voth, P. Salvador, J.J. Dannenberg, S. Dapprich, A.D. Daniels, O. Farkas, J.B. Foresman, J.V. Ortiz, J. Cioslowski, and D.J. Fox, Gaussian, Inc., Wallingford CT, 2009.

[42] E.D. Glendening, J.K. Badenhoop, A.D. Reed, J.E. Carpenter, F. Weinhold, NBO 3.1, Theoretical Chemistry Institute, University of Wisconsin, Madison, WI, 1996.

[43] B.H. Besler, K.M. Merz Jr., P.A. Kollman, Atomic charges derived from demi-empirical methods, J. Comp. Chem. 11 (1990) 431–439.

[44] F. Biegler-Köning, J. Schönbohm, D. Bayles, AIM2000; a program to analyze and visualize atoms in molecules, J. Comput. Chem. 22 (2001) 545.

[45] R.F.W. Bader, Atoms in Molecules, a Quantum Theory, Oxford University Press, Oxford, 1990. ISBN: 0198558651.

[46] S.A. Brandán, Why morphine is a molecule chemically powerful. Their comparison with cocaine, Indian J. Appl. Res. 7 (7) (2017) 511–528.

[47] P. Ugliengo, Moldraw Program, University of Torino, Dipartimento Chimica IFM, Torino, Italy, 1998.

[48] C.H.L. Kennard, G. Smithand, S. Hovmöller, 1,2,3,4,10,10-Hexaehloro-1,4,4a,5,8,8a-hexahydro-endo-1,4-endo-5,8-dimethanonaphthalene (isodrin), Acta Cryst. B 35 (1979) 493–495.

[49] N. Galešić, I. Matijašić, M. Bruvo, Structure of dimethyl 1,2,3,4,7,7-Hexachloro-5-endo-methoxybicyclo[2.2.1]hept-2-ene-5-exo,6-endo-dicarboxylate, Acta Cryst. C41 (1985) 1673–1675.

[50] M.V. Castillo, M.E. Manzur, L. Di Marco, V. Runco, S.A. Brandán, Chapter 7, Structural and vibrational study of a powerful environmental pollutant agent, the hexachlorobenzene compound, in: Silvia A. Brandán (Ed.), Descriptors, Structural and Spectroscopic Properties of Heterocyclic Derivatives of Importance for the Health and the Enviromental, Edited Collection, Nova Science Publishers, Inc., 2015, pp. 158–173. ISBN: 978-1-63482-708-9.

[51] M.V. Castillo, J.L. Pergomet, G.A. Carnavale, L. Davies, J. Zinczuk, S.A. Brandán, A complete vibrational study on a potential environmental toxicant agent, the 3,3',4,4'-tetrachloroazobenzene combining the FTIR, FTRaman, UV-Visible and NMR Spectroscopies with DFT calculations, Spectrochim. Acta 135 (2015) 577–586.

[52] M.V. Castillo, J.L. Pergomet, G.A. Carnavale, L. Davies, J. Zinczuk, S.A. Brandán, FTIR, FTRaman, UV-Visible and NMR Spectroscopic studies on 3,3',4,4'-tetrachloroazoxybenzene, an Azoxybenzene derivative with toxic effects, J. Mol. Struct. 1142 (2017) 18–27.

[53] D. Romani, S. Tsuchiya, M. Yotsu-Yamashita, S.A. Brandán, Spectroscopic and structural investigation on intermediates species structurally associated to the tricyclic bisguanidine compound and to the toxic agent, saxitoxin, J. Mol. Struct. 1119 (2016) 25–38.

[54] G. Keresztury, S. Holly, G. Besenyei, J. Varga, A.Y. Wang, J.R. Durig, Vibrational spectra of monothiocarbamates-II. IR and Raman spectra, vibrational assignment, conformational analysis and *ab initio* calculations of *S*-methyl-*N*,*N*-dimethylthiocarbamate, Spectrochim. Acta 49A (1993) 2007–2026.

[55] D. Michalska, R. Wysokinski, The prediction of Raman spectra of platinum(II) anticancer drugs by density functional theory, Chem. Phys. Lett. 403 (2005) 211–217.

[56] R. Ditchfield, Self-consistent perturbation theory of diamagnetism. I. A gage-invariant LCAO (linear combination of atomic orbitals) method for NMR chemical shifts, Mol. Phys. 27 (1974) 714–722.

[57] R.J. Abraham, M. Mobli, Modelling ^{1}H-NMR Spectra of Organic Compounds Theory, Applications and NMR Prediction Software, Wiley, Chichester, 2008.

[58] Richard H. Cox, James D. McKinney, Carbon-13 NMR spectra of some chlorinated polycyclodiene pesticides, Org. Mag. Res. 11 (1) (1978) 541–546.

[59] M. Minteguiaga, E. Dellacassa, M.A. Iramain, C.A.N. Catalán, S.A. Brandán, A structural and spectroscopic study on carquejol, a relevant constituent of the medicinal plant Baccharis trimera (Less.) DC. (Asteraceae), J. Mol. Struct. 1150 (2017) 8–20.

[60] F. Chain, M.F. Ladetto, A. Grau, C.A.N. Catalán, S.A. Brandán, Structural, electronic, topological and vibrational properties of a series of N-benzylamides derived from Maca (Lepidiummeyenii) combining spectroscopic studies with ONION calculations, J. Mol. Struct. 1105 (2016) 403–414.

[61] F. Chain, E. Romano, P. Leyton, C. Paipa, C.A.N. Catalán, M.A. Fortuna, S.A. Brandán, An experimental study of the structural and vibrational properties of sesquiterpene lactone cnicin using FT-IR, FT-Raman, UV–visible and NMR spectroscopies, J. Mol. Struct. 1065–1066 (2014) 160–169.